Kinetic Isotope Effect for H_2 and D_2 Quantum Molecular Sieving in Adsorption/Desorption on Porous Carbon Materials

Xuebo Zhao, Silvia Villar-Rodil, Ashleigh J. Fletcher, and K. Mark Thomas*

Northern Carbon Research Laboratories, School of Natural Sciences, Bedson Building, University of Newcastle upon Tyne, Newcastle upon Tyne NE1 7RU, United Kingdom

Received: February 4, 2006; In Final Form: April 1, 2006

Adsorption and desorption of H_2 and D_2 from porous carbon materials, such as activated carbon at 77 K, are usually fully reversible with very rapid adsorption/desorption kinetics. The adsorption and desorption of H_2 and D_2 at 77 K on a carbon molecular sieve (Takeda 3A), where the kinetic selectivity was incorporated by carbon deposition, and a carbon, where the pore structure was modified by thermal annealing to give similar pore structure characteristics to the carbon molecular sieve substrate, were studied. The D_2 adsorption and desorption kinetics were significantly faster (up to $\times 1.9$) than the corresponding H_2 kinetics for specific pressure increments/decrements. This represents the first experimental observation of kinetic isotope quantum molecular sieving in porous materials due to the larger zero-point energy for the lighter H_2, resulting in slower adsorption/desorption kinetics compared with the heavier D_2. The results are discussed in terms of the adsorption mechanism.

1. Introduction

Hydrogen adsorption on materials with molecular scale porosity has been proposed as a method for hydrogen storage for energy applications.[1] The hydrogen adsorbent surface interaction is weak, but is enhanced in pores with dimensions of <0.5 nm by overlap of the potential energy fields from pore walls.[2,3] Molecular transport in nanometer-sized pores differs from larger pores.[4] It has been proposed that when the difference between the diameter of the molecule and the pore diameter becomes comparable to the de Broglie wavelength (λ), quantum effects may become significant.[4−6] The de Broglie wavelengths for hydrogen and deuterium, under conditions of one-dimensional flow in nanometer cylindrical pores, at 77 K are $\sim$0.176 and 0.124 nm, respectively. Therefore, adsorption/desorption of H_2 and D_2 (size 0.24−0.31 nm) within 0.4−0.5 nm pores may involve quantum effects.

Molecular sieving occurs when molecules larger than pore dimensions are excluded from part or all of the porous structure or when there are differences in adsorption kinetics. Carbon molecular sieve (CMS) materials used for air separation are prepared by carbon deposition on a porous carbon substrate to produce kinetically selective materials, where the diffusion of oxygen into the porous structure is much faster (typically $\times 20$) than nitrogen. However, the amounts of oxygen and nitrogen adsorbed at equilibrium are similar. The kinetically selective carbon deposit is distributed heterogeneously within the porous structure and contains porosity similar in size to oxygen and nitrogen.[7−10] Heterogeneity in CMS materials was shown by the decrease in kinetic selectivity and increase in adsorption rates by particle size reduction, which results in the introduction of nonselective pathways.[10] Probe molecule studies of adsorption on a CMS used for air separation have shown that the selective porosity behaves as though it has spherical shape.[9] Size exclusion of molecules for this CMS occurs over a minimum dimension range of 0.41−0.57 nm, and the adsorption kinetics vary markedly over the molecular size range 0.3−0.41 nm.[7−9] Molecular sieving of oxygen and nitrogen is a kinetic process, following a linear driving force (LDF) model and is mainly related to differences in molecule size although other factors may be involved.[7−9] In comparison, ultra-microporous carbons may also show kinetic selectivity for oxygen and nitrogen. The adsorption kinetics for these materials, where the barriers to molecular transport are homogeneously distributed within the porous structure, follow a Fickian kinetic model.[10]

The objective of this study was to investigate the adsorption characteristics of H_2 and D_2 on porous carbons. The porous carbons used in this study were a carbon molecular sieve (CMS T3A) normally used for air separation, with selective porosity produced by carbon deposition on a porous carbon substrate and carbon (PCS), prepared by direct carbonization and thermal structural annealing of the same precursor material as CMS T3A, with very similar pore structure characteristics to the CMS T3A substrate before carbon deposition. This allowed the effects of molecular sieving in the carbon deposit and the porous substrate to be distinguished, and it also allows investigation of cases where the barriers to diffusion into the porous structure are heterogeneously (CMS T3A) and homogeneously (PCS) distributed in the carbon porous structure. In this paper, we report the discovery of a kinetic isotope effect for quantum molecular sieving in porous carbons where both the adsorption and desorption of D_2 are faster than H_2 at 77 K under the same experimental conditions. The results are discussed in relation to the adsorption/desorption mechanism.

2. Experimental Section

2.1. Materials Used. *Gases.* Ultrapure hydrogen (H_2 99.9999%, $H_2O < 500$ ppb, $N_2 < 200$ ppb, $O_2 < 100$ ppb, $CO + CO_2 < 50$ ppb, total hydrocarbons < 50 ppb) was supplied by Air Products Ltd. Deuterium (99.98% D_2), nitrogen (99.9995%), and carbon dioxide (99.999%) were supplied by BOC Ltd.

* To whom correspondence should be addressed: E-mail: mark.thomas@ncl.ac.uk.

10.1021/jp060748p CCC: $33.50
Published on Web 05/04/2006

Gas Purification. Hydrogen and deuterium were purified using a two-stage process involving adsorption on a zeolite (calcium alumino silicate (1/16" pellets)) at 298 K to remove any water vapor present and on activated carbon (G212, particle size 6 × 12 mesh) at 195 K to remove hydrocarbons and other gas impurities. The impurities were adsorbed under these conditions while little or no hydrogen or deuterium was adsorbed at 195 K. Both adsorbents were degassed at 700 K prior to use. The water adsorption isotherm for the calcium alumino silicate used at 298 K is given in Supporting Information. The isotherm is type I/II in the IUPAC classification scheme[11] with a very high Henry's law constant as shown by the isotherm in the low relative pressure range. Porous structure characterization data for G212 have been reported previously.[3]

Carbon Materials Used. Carbon molecular sieve Takeda 3A (CMS-T3A), supplied by Takeda Chemical Company, Japan, had a particle size range of 1.4−2 mm. The material was prepared by carbon deposition on a microporous substrate prepared by the carbonization of coconut shell. Initially, Takeda 3A was heat-treated under ultrahigh vacuum at 623 K for 4 h to clean and degas the sample.

The unactivated coconut shell carbon (particle size 1.4−2 mm) supplied by Pica, Vierzon, France, was heat-treated to 758 K under argon for 4 h to thermally anneal the porous structure.

2.2. Adsorption Studies. The adsorption/desorption characteristics were studied using a Hiden Analytical Intelligent Gravimetric Analyzer, which is an ultrahigh vacuum, clean system with a diaphragm and turbo pumping system.[11] This system is suitable for the measurement of adsorption kinetics in porous materials.[7−9] The microbalance had a long-term stability of ±1 μg with a weighing resolution of 0.2 μg. The sample was degassed at 543 K under ultrahigh vacuum (10^{-10} bar) until no further weight loss occurred prior to H_2 and D_2 adsorption. The approach to equilibrium was measured in real time using a computer algorithm. The pressure was monitored by three pressure transducers with ranges 0−0.2, 0−10, and 0−100 kPa and maintained at the set point by active computer control of inlet/outlet valves throughout the duration of the adsorption kinetic experiments. The accuracy of the set-point pressure regulation was ±0.02% of the range used. Both the sample and counterweight sides of the balance were cooled to 77 K for the H_2 and D_2 adsorption/desorption experiments in order to minimize buoyancy corrections and thermal transpiration effects.

The major problem with studying H_2 and D_2 adsorption and desorption is the adsorption of impurities from both the adsorptive gas used and within the UHV system. The measurement protocols used in this study were validated by the complete desorption of H_2 and the absence of marked hysteresis in the isotherms measured for CMS-T3A, PCS, and G212.[3] The validity of the uptake measurements was further confirmed by isobar data on G212, which were corrected for changes in buoyancy effects as a function of temperature.[3] Measurements of the isosteric enthalpy of adsorption at zero surface coverage using the virial equation showed that it did not vary with temperature, which is consistent with thermodynamic considerations.[3] Measurements of the isosteric enthalpy of adsorption using the van't Hoff isochore method were in good agreement with those obtained from the virial method.

The adsorption of impurities is evident if there is a very slow uptake after initial equilibrium. The worst case scenario for these studies was adsorption at 100 kPa hydrogen pressure. Long-term tests showed that the uptake changed by <0.1% over 900 min after equilibrium had been achieved. This verifies that adverse effects of impurity adsorption were not observed and demonstrates the long-term stability of the equipment.

The repeatabilities of the isotherm and kinetic measurements were established by a detailed series of measurements on both CMS-T3A and PCS, and these are discussed in the Results Section.

Saturated Vapor Pressures. Hydrogen, deuterium, and nitrogen were used above their critical temperatures. The saturated vapor pressures for carbon dioxide were calculated using the following equation[12]

$$\log_{10} p = A - \frac{B}{T + C} \tag{1}$$

where p is the saturated vapor pressure (Torr), T is the temperature in degrees Celsius, and A, B, and C are constants defined by the adsorbate carbon dioxide (77−303 K): $A = 7.810237$, $B = 995.7048$, $C = 293.4754$.

3. Results and Discussion

3.1. Porous Structure Characterization. Both CMS T3A and PCS did not adsorb significant amounts of nitrogen at 77 K because of activated diffusion effects. Therefore, the porous structure was characterized using carbon dioxide adsorption at 195 and 273 K, and all the isotherms were type 1 in the IUPAC classification scheme.[13]

The micropore volumes of the carbons were obtained using the Dubinin−Radushkevich (DR) equation, which is as follows:

$$\log n = \log n_0 - D \log^2(p^0/\mathrm{p}) \tag{2}$$

where n is the amount adsorbed, n_0 the amount adsorbed corresponding to the micropore volume, p the pressure, p^0 the saturated vapor pressure, and D is a constant related to the microporous structure of the adsorbent.[14] The DR graphs for the carbon dioxide adsorption data for both CMS T3A and PCS at 273 K are linear and have very similar gradients (see Supporting Information). These adsorption methods and analysis using the DR equation give micropore volumes for pore sizes $\lesssim 0.7$ nm.[15−17] The micropore volumes for CMS T3A and PCS, calculated using an adsorbate density of 1.023 g cm^{-3}, were 0.224 ± 0.001 and 0.178 ± 0.001 cm^3 g^{-1}, respectively The mean radii of microporosity from the Dubinin−Stoeckli correlation method[18] of CO_2 adsorption data at 273 K were very similar with values of 0.273 and 0.283 nm for CMS T3A and PCS, respectively. It is apparent that both carbons have similar mean pore size.

The total pore volumes can be assessed from amounts adsorbed at the maximum relative pressure ($p/p^0 = 0.98$) measured for the carbon dioxide adsorption isotherm data obtained at 195 K or by extrapolating the data to $p/p^0 = 1$ using a suitable model which describes the isotherm accurately. The Langmuir equation can be expressed in the following form:[19]

$$p/n = 1/n_{\mathrm{m}}b + p/n_{\mathrm{m}} \tag{3}$$

where p is the pressure, n the amount adsorbed, n_{m} is the monolayer capacity, and b is the coefficient of adsorption specific to the adsorbate/adsorbent system. The total pore volumes obtained from the Langmuir isotherm model using a density of 1.023 g cm^{-3} for the adsorbed phase were 0.2289 ± 0.0014 and 0.212 ± 0.003 for cm^3 g^{-1} CMS T3A and PCS, respectively (see Supporting Information). These pore volume values agree well with isotherm uptakes at $p/p^0 = 0.98$ of 5.272 and 4.91 mmol g^{-1} for CMS T3A and PCS, respectively. These

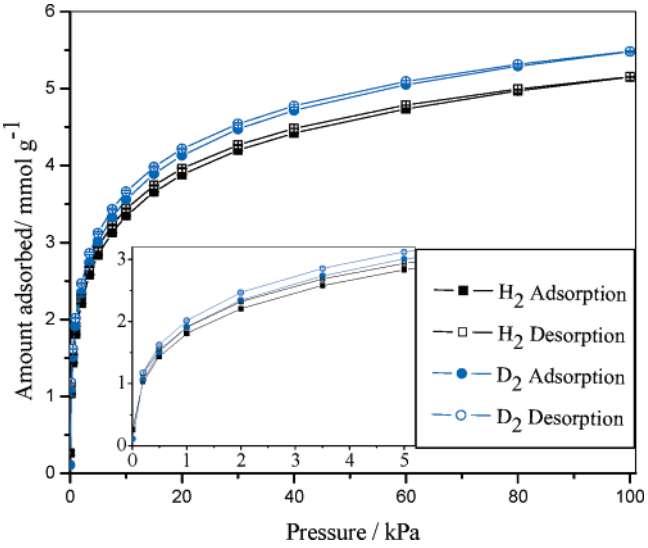

Figure 1. Adsorption and desorption isotherms for H_2 and D_2 on CMS T3A at 77 K. Isotherms are an average of three runs. The low-pressure range is inset to show the differences in this region.

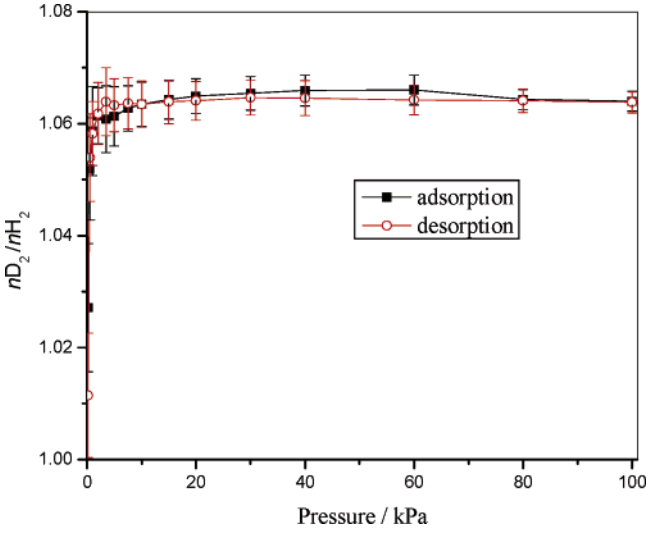

Figure 2. Variation of the ratio of the amounts adsorbed (nD_2/nH_2) for H_2 and D_2 adsorption and desorption isotherm points on CMS T3A with pressure at 77 K.

amounts adsorbed correspond to adsorbate volumes of 0.227 and 0.211 $cm^3\ g^{-1}$ for CMS T3A and PCS, respectively.

The results from the adsorption of carbon dioxide at 195 and 273 K show that both CMS T3A porous substrate and PCS have very similar pore structure characteristics since the carbon deposition, which is the kinetic selective material for air separation in CMS T3A, only represents ~1 wt % of the material, and therefore, any contribution to the isotherm is minimal.

3.2. H_2 and D_2 Adsorption Isotherms. Figure 1 shows the adsorption and desorption isotherms for purified H_2 and D_2 on CMS T3A at 77 K. The repeatabilities of the amounts adsorbed (n) for isotherm points averaged ±0.20% for adsorption and ±0.23% desorption, respectively, for H_2 over the pressure (p) range 0.2−100 kPa. The corresponding repeatabilities for D_2 adsorption and desorption isotherm points were ±0.39 and ±0.33%, respectively. The largest errors for isotherm points were at low pressure (0.2 kPa), and these were ~0.79% for H_2 and D_2 adsorption and 0.57% for H_2 and D_2 desorption, respectively.

Both isotherms are type I in the IUPAC classification scheme[13] and show a very small amount of hysteresis, which increases with decreasing pressure similar to kinetically nonselective activated carbons.[3] The hysteresis for H_2 and D_2 is compared in a graph of the difference between adsorption and desorption for D_2 versus H_2 (Supporting Information). The graph is linear with a 1:1 correspondence on a mole basis.

Carbon PCS also had type I H_2 and D_2 adsorption/desorption isotherms but with slightly lower amounts of H_2 and D_2 adsorption compared with CMS T3A. The repeatabilities of the amounts adsorbed (n) for isotherm points averaged ±0.73 and 0.46% for adsorption of H_2 and D_2 over the pressure (p) range 0.2−5 kPa, respectively. The largest errors for isotherm points were at low pressure (0.2 kPa), and these were ±1.38 and ±0.73% for H_2 and D_2 adsorption, respectively. These values are similar to those obtained for CMS T3A.

Comparison of the molar D_2/H_2 ratios (nD_2/nH_2) for specific adsorption points in Figure 2 showed that they did not change markedly with pressure in the range 0.5−100 kPa and averaged 1.063 ± 0.004 for CMS T3A (see Figure 2) and 1.097 ± 0.009 for the nonkinetically selective carbon PCS (see Supporting Information). These values compare with an average nD_2/nH_2 ratio for specific isotherm points for a nonselective activated carbon (G212), with fast adsorption kinetics, over the same pressure range, of 1.076 ± 0.006.[3] The desorption isotherms for CMS T3A and PCS showed similar trends for the nD_2/nH_2 ratios. Previous studies have also shown slightly larger amounts of D_2 adsorbed compared with H_2 adsorbed on carbons under the same conditions.[20, 21]

Therefore, there is no evidence for exclusion of H_2 or D_2 by the selective porosity in CMS T3A.

3.3. Langmuir Isotherms. The critical temperatures of H_2 and D_2 are 32.97 and 35.34 K, and a saturated vapor pressure is not obtainable for calculation of a relative pressure for adsorption above these temperatures. Therefore, the isotherm models that can be used for H_2 and D_2 adsorption data at 77 K are limited. Langmuir isotherms for H_2 and D_2 adsorption on CMS T3A were linear over the pressure range 20−100 kPa (see Supporting Information), and the maximum amounts adsorbed (n_m) obtained from these graphs were 5.62 ± 0.08 and 5.98 ± 0.08 mmol g^{-1} for PCS and CMS T3A, respectively. The Langmuir isotherms for H_2 and D_2 adsorption on PCS were similar, and the maximum amounts adsorbed (n_m) obtained from these graphs were 5.42 ± 0.07 and 5.87 ± 0.08 mmol g^{-1}, respectively. The ratios n_mD_2/n_mH_2 for CMS T3A and PCS were 1.064 and 1.084, respectively. These ratios are consistent with average nD_2/nH_2 ratios for specific isotherm points given in the previous section.

When the H_2 and D_2 isotherms are plotted as n/n_m versus pressure (p), i.e., as fractional surface coverage versus pressure; they overlap very closely for both CMS T3A and PCS, as shown in Figure 3. This indicates that H_2 and D_2 adsorption on both CMS T3A and PCS have very similar isotherms. A correlation between hydrogen volume adsorbed and micropore volume has been observed.[3,22] The values for n_m for hydrogen adsorption can be converted to a volume of adsorbate using the density of adsorbed hydrogen at the triple point of 0.077 g cm^{-3},[12] and these values show a good correlation with the micropore volume for a wide range of functionalized carbons.[3] The values for PCS and CMS T3A fit on this correlation (see Supporting Information). These results suggest that only the micropore volume in carbons is filled by adsorbed hydrogen.[3] The micropore volume can be converted to surface area, and hence the correlation is consistent with the one between hydrogen adsorbed and surface area.[23]

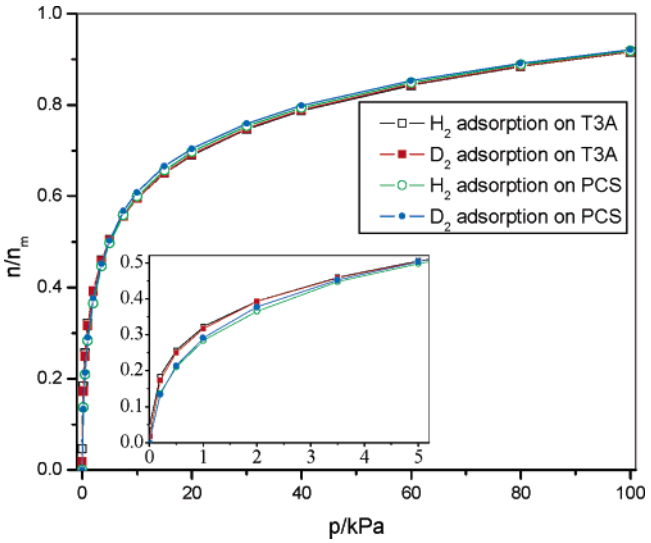

Figure 3. Comparison of adsorption isotherms for H_2 and D_2 adsorption on CMS T3A and PCS at 77 K on a surface coverage (n/n_m) basis. The low-pressure range is inset to show the differences in this region.

The density of adsorbed hydrogen calculated from n_m and the total pore volume was in the range 0.050−0.052 g cm^{-3} for PCS and CMS T3A. The corresponding range of adsorbed phase density values obtained using micropore volumes was 0.051−0.061 g cm^{-3}. The ranges are similar to adsorbed hydrogen density values obtained previously,[3] and the density of liquid hydrogen is 0.0708 g cm^{-3} at 20.2 K.[12] Deuterium is adsorbed to a greater extent than hydrogen on a mole basis, and therefore, the adsorbed D_2 phase has a higher molar density than H_2. It is known that liquid D_2 has a higher density than liquid H_2 on a mole basis.[12]

3.4. Virial Graphs. Analysis of the isotherm data was performed using the virial equation[3,24]

$$\ln(n/p) = A_0 + A_1 n + A_2 n^2 ... \quad (4)$$

where A_0, A_1, etc. are virial coefficients. A_0 is related to adsorbate−adsorbent interactions, whereas A_1 describes adsorbate−adsorbate interactions. The Henry's law constant (K_H) is equal to exp(A_0). The virial graphs for H_2 and D_2 adsorption on CMS T3A at 77 K are shown in Figure 4, and the corresponding virial graphs for PCS are given in Supporting Information. It is apparent that the graphs are linear. The virial parameters for both CMS T3A and PCS are given in Table 1. The values of A_0 and A_1 are similar to those obtained previously for hydrogen adsorption on a wide range of carbons[3] at 77 K while the values for A_1 are also similar to those obtained for adsorption of a range of gases (nitrogen, carbon dioxide, etc.) on a carbon molecular sieve over the temperature range 303−343 K.[7−9] Virial parameters A_0 and A_1 are less negative for D_2 than for the corresponding H_2 adsorption for both CMS T3A and PCS. A_0 for D_2 adsorption is $\sim 3\sigma$, , where σ is the standard deviation, different from H_2 adsorption on PCS while the corresponding difference is $\sim 1\sigma$ for CMS T3A. Since these differences for H_2 and D_2 adsorption are consistent for both materials it suggests that K_H is higher for D_2, indicating slightly stronger adsorbate−adsorbent interactions for D_2. The A_1 values for D_2 adsorption are $\sim 7-8\ \sigma$ lower than those for H_2 adsorption for both CMS T3A and PCS. These differences are statistically significant indicating that adsorbate−adsorbate interactions are lower for D_2 adsorption. The slightly higher K_H for D_2 adsorption compared with H_2 adsorption is consistent with the

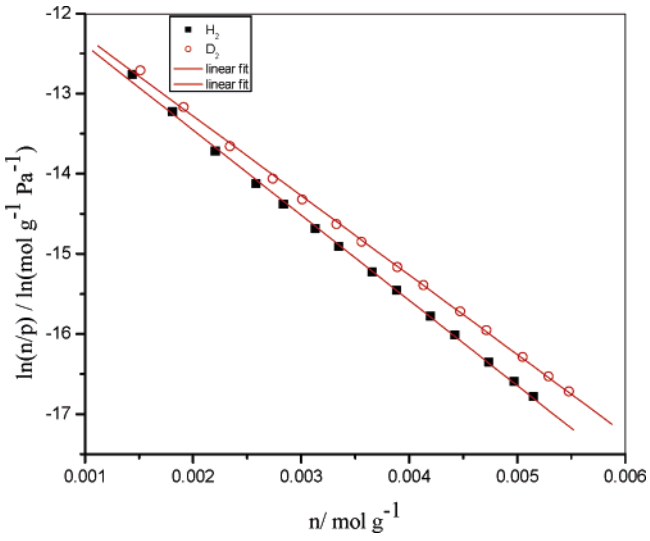

Figure 4. Virial Graphs for H_2 and D_2 adsorption on CMS-T3A at 77 K.

TABLE 1. Virial Parameters for Adsorption of H_2 and D_2 on CMS T3A and Carbon PCS at 77 K

adsorbent	adsorbate	K_H/ mol g^{-1} Pa^{1-}	A_0/ ln(mol g^{-1} Pa^{-1})	A_1/ g mol^{-1}
CMS T3A	H_2	1.206×10^{-5}	-11.326 ± 0.034	-1063.9 ± 9.4
CMS T3A	D_2	1.243×10^{-5}	-11.295 ± 0.032	-992.4 ± 8.3
PCS	H_2	7.075×10^{-6}	-11.859 ± 0.035	-962.5 ± 12.0
PCS	D_2	7.795×10^{-6}	-11.762 ± 0.015	-879.0 ± 10.0

higher value of n_m obtained from the Langmuir isotherms and may be attributed to competing quantum effects: (1) the quantum-statistical mass effect on the vibrational energy levels normal to the surface and (2) the quantum-mechanical effect of isotopic substitution on the dispersion energy.[20,25] The differences in A_1 indicate higher adsorbate−adsorbate interactions, which imply higher repulsion energies between neighbors for H_2 than for D_2. This is related to the larger zero-point energy of H_2 compared with D_2.

3.5. H_2 and D_2 Adsorption and Desorption Kinetics. Figure 5 shows adsorption/desorption profiles for a typical isotherm pressure increment/decrement for both H_2 and D_2 at 77 K. The rates of adsorption and desorption for D_2 are faster than the corresponding profiles for H_2. The kinetic profiles can be described by a stretched exponential (SE) model:[26]

$$\frac{M_t}{M_e} = 1 - e^{-(kt)^b} \quad (5)$$

where β is the exponential parameter of the adsorption/desorption process, which covers the range $0.5 < \beta < 1$. The value of β gives an indication of the dimensions involved in the adsorption process. When $\beta = 0.5$, the process is one-dimensional with a distribution of relaxation times while $\beta = 1$ for a three-dimensional process with a single relaxation time. The latter is the linear driving force model, which is a nested model of the SE model and is obeyed for O_2 and N_2 adsorption on CMS T3A. Typical comparisons of the residuals from fitting the SE model to the experimental data are given in Figure 6. The model fits the experimental data with residuals in the range ±0.02 over the normalized uptake profiles. The repeatabilities of the rate constants obtained from the stretched exponential model averaged ±2% for both H_2 and D_2 adsorption and ±3.5% for both H_2 and D_2 desorption on CMS T3A. The repeatabilities of the individual exponential (β) values obtained from the

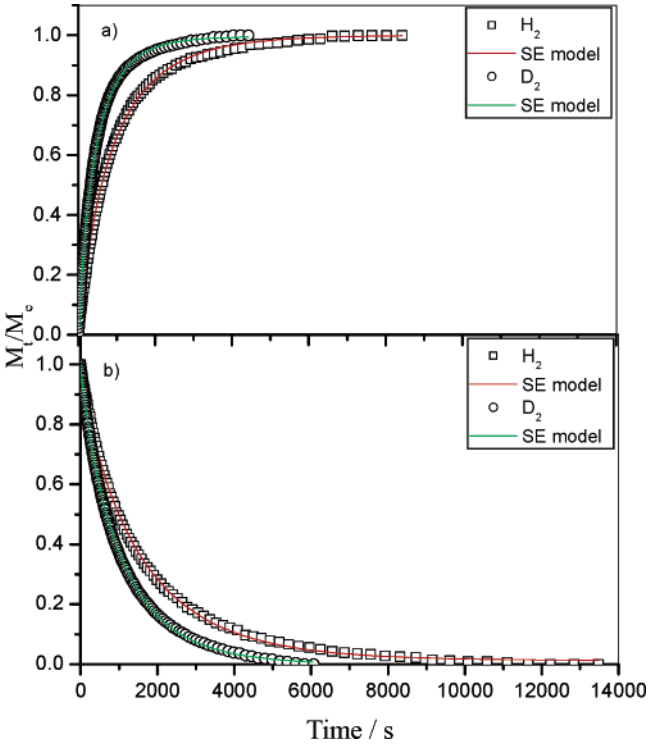

Figure 5. Typical H_2 and D_2 adsorption and desorption kinetic profiles for pressure increments (1−2 kPa) and decrements (2−1 kPa) on CMS T3A at 77 K: (a) adsorption and (b) desorption.

stretched exponential kinetic model for H_2 and D_2 adsorption and desorption averaged ±2%.

Figure 7 shows the variation of rate constants for H_2 and D_2 adsorption and desorption on CMS T3A, obtained from the SE model, with pressure. The rate constants for both adsorption and desorption increase with increasing pressure, and the D_2 adsorption and desorption rate constants are faster than the corresponding H_2 parameters. The variation of β values with pressure for H_2 and D_2 adsorption are shown in Figure 8. The values do not vary significantly over the pressure range 0.5−100 kPa with $\beta = 0.918 \pm 0.009$ and 0.909 ± 0.025 for H_2 and D_2 adsorption, respectively. In contrast, β for desorption of H_2 and D_2 from CMS T3A decreases with decreasing pressure. However, for both H_2 and D_2 adsorption and desorption on CMS T3A, the β values for a given pressure increment/decrement are not significantly different. The observed differences in the rates of adsorption and desorption can be described solely by the rate constants.

The kinetics for H_2 and D_2 adsorption and desorption on carbon PCS were much faster than for CMS T3A under similar experimental conditions because of the absence of the kinetically selective carbon deposit in PCS. The adsorption kinetics of H_2 and D_2 on PCS were only studied in detail at pressures up to 5 kPa where marked differences were observed. The repeatabilities of the rate constants obtained from the stretched exponential model averaged ±2.6 and ±2.9% for both H_2 and D_2 adsorption, respectively. The repeatabilities of the exponent (β)) values obtained from the stretched exponential kinetic model for H_2 and D_2 adsorption averaged ±2.1 and 2.8%, respectively. The rate constants for both adsorption and desorption of D_2 and H_2 on PCS show similar trends with change in pressure to CMS T3A. The β values were in the range 0.75−0.82 and 0.78−0.85 for H_2 and D_2 adsorption, respectively. These values are lower than those for CMS T3A under the same conditions, and this represents rate-determining diffusion through barriers with a wider range of pore sizes than CMS T3A in which diffusion

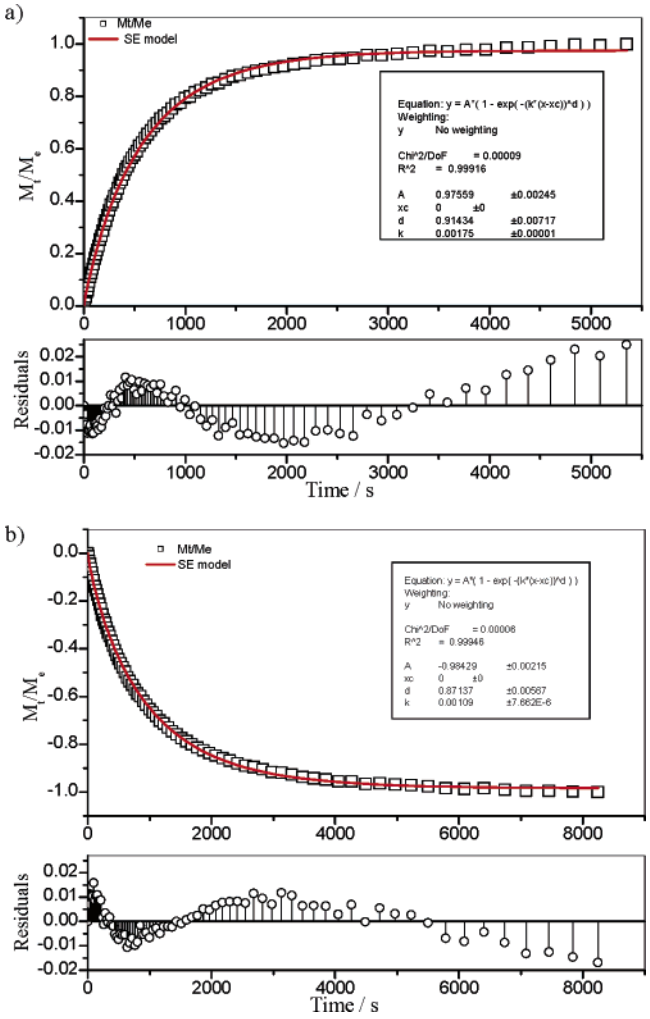

Figure 6. Kinetic profiles for H_2 adsorption/desorption on CMS T3A and stretched exponential model fit for (a) pressure increment 2−3.5 kPa and (b) pressure decrement 3.5−2 kPa.

through the carbon deposit is the rate-determining process. The β values increased slightly with increasing pressure. This weak trend contrasts with that for CMS T3A.

3.6. Comparison of H_2 and D_2 Adsorption/Desorption Characteristics. The ratios of rate constants kD_2/kH_2 for CMS T3A and PCS decrease with increasing pressure for both adsorption and desorption as shown in Figure 9. The results show that D_2 adsorption kinetic rate constants were ×1.9 faster than the corresponding H_2 rate constants (pressure range 0−5 kPa) and decreased with increasing pressure above 5 kPa to ∼1.1 at 50 kPa. Figure 10 shows that the kD_2/kH_2 ratio was ∼×1.9 for surface coverage 0−0.5 n/n_m for CMS T3A. The kD_2/kH_2 ratios for pressure increments for PCS were 1.25−1.07 for adsorption over the pressure range 0−5 kPa (0−0.5 n/n_m) and decrease with increasing pressure similar to CMS T3A. Hence, the two carbons, CMS T3A and PCS, with the narrowest porosity produced by different methods have ratios of rate constants $kD_2/kH_2 > 1$, and hence, D_2 adsorption/desorption is faster than H_2. The results indicate that kD_2/kH_2 is dependent on pressure and surface coverage as well as pore size. Measurements of the kinetic barriers for hydrogen and deuterium adsorption/desorption on CMS T3A and PCS could not be obtained because of the difficulty in controlling the temperature to ±0.05 K at temperatures other than 77 K and the rapid decrease in the amount of hydrogen adsorbed with increasing temperature.[3]

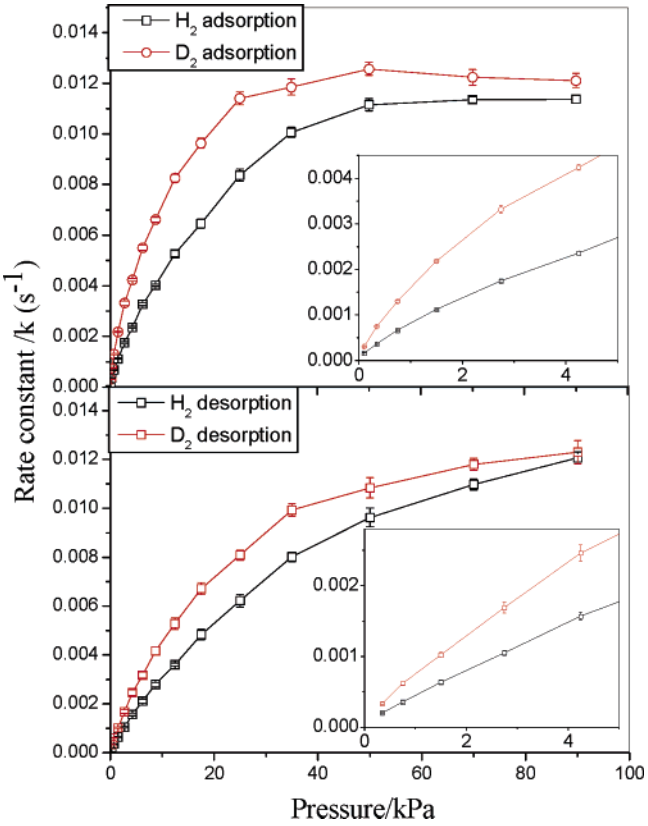

Figure 7. Variation of rate constants for H_2 and D_2 adsorption and desorption on CMS T3A at 77 K obtained from the stretched exponential model with pressure: (a) adsorption and (b) desorption. The average pressure for the pressure increment/decrement is used in the figure. The low-pressure range is inset to show the differences in this region.

Carbon PCS has similar H_2 and D_2 adsorption/desorption isotherms to CMS T3A on a surface coverage basis (see Figure 3). However, the adsorption kinetic rate constants for H_2 and D_2 for specific pressure increments are always much faster for PCS than for CMS T3A while the parameters show the same trend as for CMS T3A. The kinetic barriers to diffusion into CMS T3A and PCS materials were compared using nitrogen, argon, and carbon dioxide as probe molecules. In all cases, adsorption of the molecules was much faster for PCS than CMS T3A. Nitrogen adsorption was investigated in detail, and the activation energies for diffusion at zero surface coverage were determined (see Supporting Information). The activation energy for adsorption of nitrogen on CMS T3A was much higher (32.33 $\pm$ 0.26 kJ mol^{-1}: temperature range 273−323 K) compared with that on PCS (6.02 $\pm$ 0.94 kJ mol^{-1}: temperature range 262−276 K). The activation energy for CMS T3A was slightly lower than that of 43.5 $\pm$ 0.3 kJ mol^{-1} (temperature range 303−343 K) obtained for CMS A, a similar carbon molecular sieve material used for air separation.[8] Since the rate constants for hydrogen, deuterium, carbon dioxide, and argon are all much faster for PCS than for CMS T3A, the same order for the kinetic barriers for the molecules is expected. The kinetic barrier is much higher in CMS T3A, and this corresponds to diffusion through kinetically selective carbon deposit material, which gives slower rate constants for CMS T3A than for PCS for the same pressure increments and higher ratios of kD_2/kH_2, indicating a relationship between the kinetic barriers and the isotope kinetic selectivity.

3.7. Molecular Transport into Porous Materials. Diffusion of H_2 and D_2 into porous materials may involve surface,

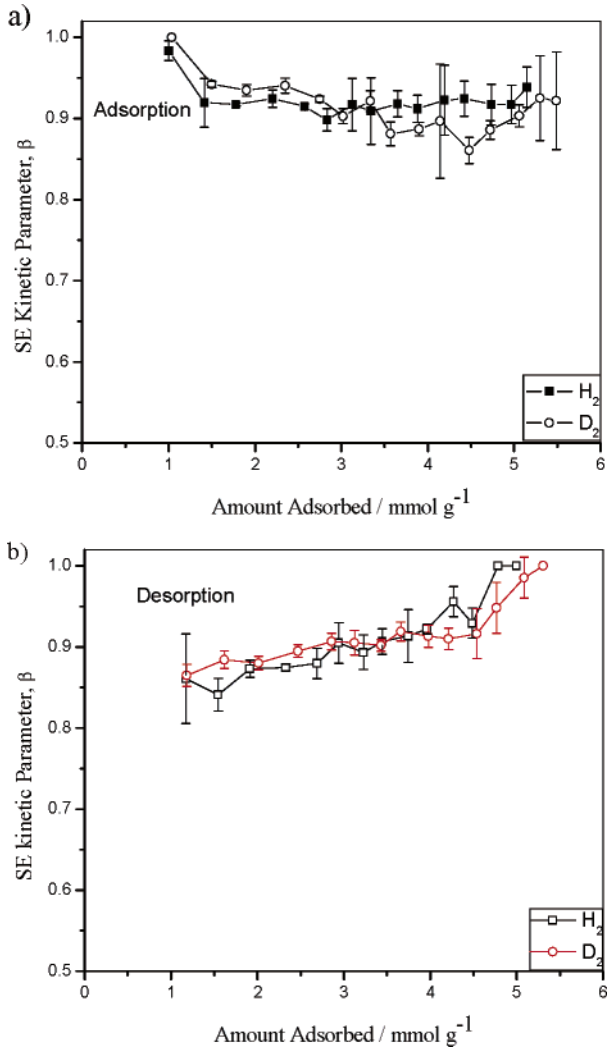

Figure 8. Variation of stretched exponential parameter β with amount adsorbed for H_2 and D_2 adsorption/desorption on CMS-T3A at 77 K: (a) adsorption and (b) desorption.

Knudsen, and gas-phase diffusion depending on the mean free path of the species relative to pore widths. The mean free paths (λ_{mfp}) were calculated, using data on collision diameters,[27] from the following equation:

$$\lambda_{mfp} = \frac{RT}{\sqrt{2}\pi d^2 N_A P} \qquad (6)$$

where P is the pressure, T is the temperature in Kelvin, R is the gas constant, d is the collision diameter, and N_A is Avogadro's constant. The minimum values of λ_{mfp} for the systems used in this study occur at 1 bar pressure. These calculations using 0.27 nm as a collision diameter gave minimum values for λ_{mfp} of $\sim$33 nm for both H_2 and D_2. Therefore, only the surface diffusion mechanism needs to be considered.

Rao et al. developed a model[28] for the interaction potential of diffusing species in pores in CMS based on the previous model for the interaction of gases with carbon surfaces.[29] Two processes are involved: (a) diffusion along the pores and (b) diffusion through the barriers at pore entrances. An LDF model is followed when the latter is the rate-determining step and this is the case for adsorption of argon, nitrogen, and carbon dioxide on CMS materials, such as T3A, with kinetic selectivity incorporated by carbon deposition. These materials lose their selectivity for nitrogen and oxygen when the particle size is

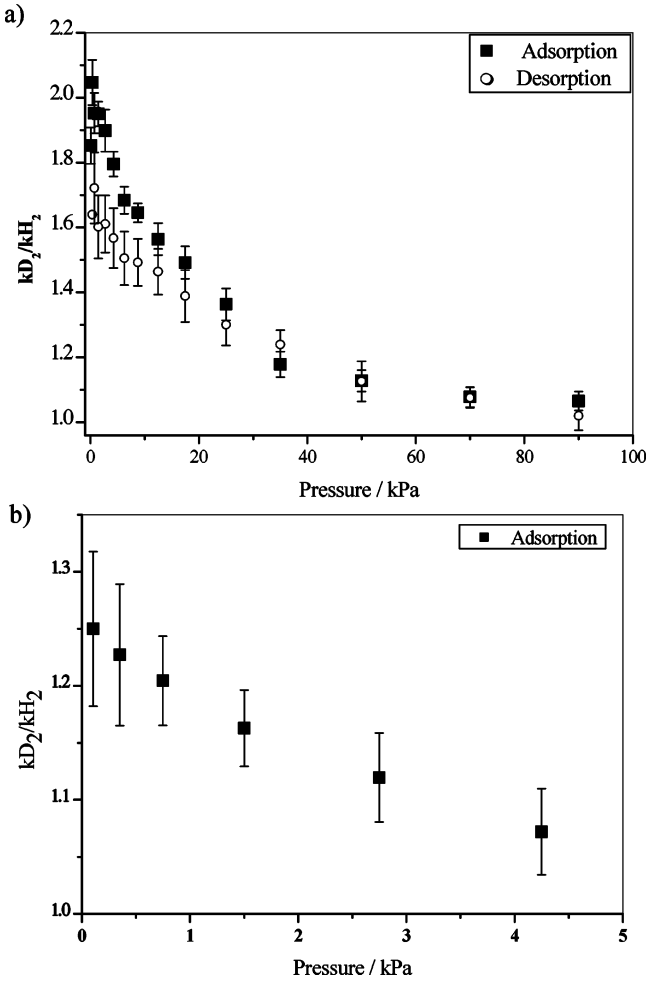

Figure 9. Variation of the ratio of the rate constants for H_2 and D_2 adsorption (solid symbol) and desorption (open symbol) with pressure at 77 K on (a) CMS T3A and (b) PCS.

reduced because it results in the introduction of nonselective pathways.[10] In the case where kinetics are controlled by diffusion along the pores, a Fickian model has been observed. Intermediate cases can be described by either a stretched exponential model or a combined barrier resistance/Fickian diffusion model.[30]

In the gas phase, both H_2 and D_2 have bond lengths of 74.16 pm, and this is consistent with the classical description of isotopes.[31] Therefore, separation on the basis of size alone is not possible. There are small differences in the compositions of the *ortho* and *para* spin isomers with H_2 having 75% *ortho* form[32] whereas D_2 has 67% at 77 K.[33] However, the isotherms and kinetic profiles did not show characteristics attributable to *ortho* and *para* forms of H_2 and D_2.

Studies of H_2 and D_2 adsorption on charcoal gave values in the range of approximately 7−1.5 kJ mol^{-1} for the enthalpies of adsorption, which decreased with increasing surface coverage.[21] The enthalpies of D_2 adsorption were slightly higher (∼0.75 kJ mol^{-1}) than for H_2 adsorption. Similar values of 5.4 and 5.6 kJ mol^{-1} were obtained for the isosteric enthalpies of adsorption at zero surface coverage for H_2 and D_2 on a graphitized carbon black over the temperature range 90−138 K, respectively.[25] These results are consistent with the order for Henry's law constants in Table 1. The A_0 and A_1 virial parameters for adsorption of a range of gases on CMS A were very similar to CMS T3A and correlate with the isosteric enthalpy of adsorption (Qst) at zero surface coverage.[9] A_0 increases with increasing isosteric enthalpy at zero surface coverage (Qst$_0$). Therefore, the larger value of the Henry's law constant (K_H) ($K_H = \exp(A_0)$) is consistent with a higher Qst$_0$.[9] The virial parameters, A_0 and A_1, for both CMS T3A and carbon PCS indicate that the adsorbate−adsorbent interaction is slightly stronger, and the adsorbate−adsorbate repulsive interactions are weaker for D_2 than for H_2 adsorption.

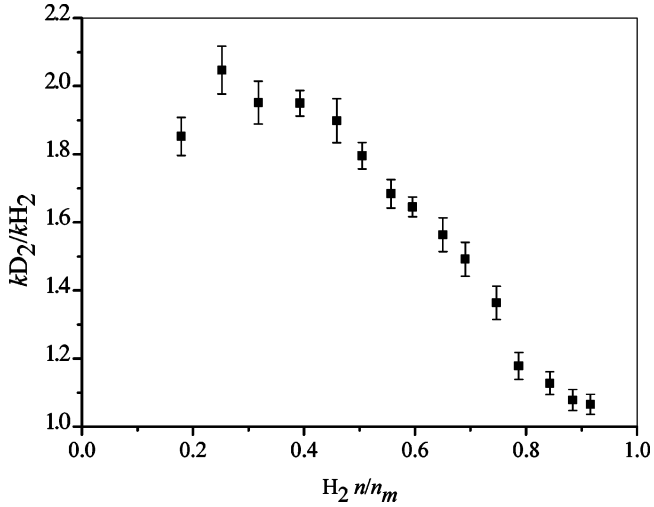

Figure 10. Variation of the ratio of the rate constants for H_2 and D_2 adsorption (kD$_2$/kH$_2$) with surface coverage for CMS T3A at 77 K.

The adsorption of D_2 on charcoal over the temperature range 55−90 K was ∼8% greater than that of H_2, whereas in the range 17−20 K the difference was 15%. Similar values of 6−9% greater D_2 than H_2 adsorption at 77 K were reported for graphitized carbon blacks and activated carbons.[3,20,21] The former is very similar to the values obtained in this study at 77 K and indicate that there is no evidence for preferential exclusion of either H_2 or D_2 from the porous structure.

The H_2 and D_2 isotherms for CMS T3A and PCS overlap when plotted as n/n_m. These observations are consistent with the higher zero-point energy for H_2 compared with D_2. The density of adsorbed hydrogen is not known. Studies of hydrogen adsorption at 77 K on single-walled nanohorns (SWNHs) suggested that the density of adsorbed hydrogen inside SWNHs was lower than that of liquid hydrogen, and this was ascribed to quantum effects.[34]

Since the molecular sizes of H_2 and D_2 are the same in the gas phase and the latter is heavier, diffusion of D_2 along the pores is expected to be slower ($\times 1/\sqrt{2}$ H_2 rate for Knudsen diffusion) than that of H_2. Probe molecule studies have shown that the selective porosity in the carbon deposit in CMS materials behaves as though it has a spherical shape, and the adsorption kinetics decrease with increasing cross-section size in the range 0.3−0.4 nm.[9] Size exclusion of molecules with dimensions in the range 0.4−0.5 nm was observed, and this is the pore size of the kinetically selective material. This range is smaller than the average value for the CMS T3A carbon substrate of 0.546 nm (see Section 3.1). In the selective porosity, the radial degrees of freedom are restricted to one dimension, and the de Broglie wavelengths for hydrogen and deuterium are ∼0.176 and 0.124 nm at 77 K, respectively. This leads to quantum effects when the molecule and pore dimensions are similar, and the zero-point energy overcompensates for the attraction of the pore walls resulting in an energy barrier at the pore entrance. This barrier is greatest for the molecule with the highest zero-point energy. Therefore, while the sizes of H_2 and D_2 are the same in the gas phase, the barrier to entry to the pores is greatest for H_2 due to higher zero-point energy. Beenakker et al. predicted on the basis

of a hard sphere/pore model, which did not take into consideration molecule−molecule interactions, that this would lead to exclusion of H_2 from the porous structure due to the higher barrier related to the higher zero-point energy of H_2 compared with D_2.[5] Recent studies of modeling equilibrium isotherms using more realistic models have also indicated that D_2 is selectively adsorbed compared to H_2.[35−37] More detailed multicomponent path integral grand canonical Monte Carlo simulations of quantum effects for the adsorption of isotopes on carbon nanotubes have also been used to investigate equilibrium separation characteristics.[37−39] These calculations refer to model systems rather than real systems where experimental data have been obtained and also indicate the selective adsorption of D_2 over H_2. The predictions from mixture simulations showed reasonable agreement up to moderate surface coverage with predictions based on ideal adsorption solution theory (IAST).[38] Quantum isotope effects were also proposed for adsorption on porous metal organic framework materials.[40]

Atomistic molecular dynamics simulations incorporating quantum effects via the Feynman−Hibbs approach were used to study H_2 and D_2 adsorption in zeolite rho.[41] The narrowest porosity in rho has an elliptical shape with minimum size of 0.543 nm. Simulations of transport of H_2 and D_2 through these pores shows that quantum effects reduce diffusivity of the adsorbate fluid confined in pores, in contrast to bulk fluids, where quantum effects have been shown to increase self-diffusivity of water.[43] The increase in quantum diffusivity over classical in bulk fluids has been attributed to quantum tunneling. Fluid−solid interactions are temperature independent for a classical fluid but temperature dependent for a quantum fluid, with the lighter H_2 having the largest effect due to its smaller mass. The molecular simulation studies of diffusivity of H_2 and D_2 in zeolite rho pores indicated that the decreased well depth for H_2 was associated with an increase in the effective size parameter for adsorbate−adsorbate and adsorbate−adsorbent quantum interactions. The hardness of the adsorbate−adsorbent interaction as shown by the slope of the repulsive region of the potential curve was also higher for H_2 compared with D_2. An increase in diffusivity is expected from a decrease in potential well depth and increased hardness of the repulsive part of the potential curve. However, the dominant effect was shown to be the increase in effective size parameter for the adsorbate−adsorbent interactions for H_2 compared with D_2.

The average pore diameter values of 0.546 and 0.566 nm obtained in this study for the CMS T3A substrate and PCS are similar to zeolite rho used in the simulation study described above. Diffusion of nitrogen (molecular dimensions: $0.2991 \times 0.3054 \times 0.4046$ nm)[42] through the selective porosity in CMS T3A gives a net repulsive force upon entering the very narrow selective pores resulting in a kinetic barrier of $\sim$32 kJ mol^{-1}. This is due to the interaction of nitrogen with the potential energy fields of the selective porosity. In contrast, H_2 and D_2 are smaller in classical dimensions ($0.24 \times 0.24 \times 0.31$ nm based on van der Waals radii and bond length) but are subject to quantum effects. The difference in the effective size parameters for H_2 and D_2 are apparent from greater adsorbate−adsorbate interactions for H_2 shown by comparison of the A_1 virial parameters (see Table 1) and the normalization of the isotherms on a surface coverage basis (see Figure 3). The slightly greater D_2−surface interaction compared with H_2 is shown by comparison of the A_0 virial parameters and the isotherms. The quantum effects for D_2 are weaker than for H_2.

The experimental work reported in this study demonstrates unequivocally the kinetic quantum molecular sieving for D_2 and H_2 in the absence of differences in equilibrium adsorption for CMS T3A compared with nonkinetically selective carbons. Exclusion of H_2 from the porous structure predicted by the simulations was not observed in this study. However, taking into consideration the sizes of the molecules are the same and the amplitudes of vibration of atoms, a sharp cutoff is not anticipated and an intermediate region, where kinetic effects are observed, may be expected. The slower adsorption/desorption kinetics for H_2 compared with that for D_2 is due to diffusion through the barrier in the selective porosity in CMS T3A and constrictions in the pore structure in PCS. These are the rate-determining steps. The decrease in k_{D_2}/k_{H_2} at high surface coverage ($n/n_m > 0.5$) is due to increased adsorbate−adsorbate interactions. In addition, a higher k_{D_2}/k_{H_2} ratio was observed for CMS T3A than PCS, and this follows the order of slower kinetics which is related to the higher kinetic barriers in CMS T3A compared with PCS as shown by probe molecule studies. This suggests that the higher quantum molecular sieving is associated with a higher kinetic barrier and narrower selective porosity in the rate-determining diffusion into the porous structure. In situ inelastic neutron scattering studies of H_2 adsorbed on single-wall nanotubes suggest that the H_2 bond is longer when adsorbed on the surface, and this is due to overcompensation of the zero-point energy.[44] The liquid densities of hydrogen isotopes vary significantly with temperature but the following data are available: H_2, 35.12 mol L^{-1} at 20.14 K;[12] D_2, 41.9 mol L^{-1} at 22.24 K;[12] T_2, 45.39 mol L^{-1} at 20.61 K.[45] These data show that the liquid densities of the isotopes on a mole basis are in the order $T_2 > D_2 > H_2$. A similar explanation of the zero-point energy overcompensation for the van der Waals forces is an explanation for the fact that H_2 is significantly less dense than liquid D_2 on a mole basis and has a significant impact on the adsorption characteristics since the adsorbed phase has similar characteristics at high surface coverage. Quantum effects may also contribute to selectivity for adsorption of other gases such as oxygen and nitrogen on carbon molecular sieves.

4. Conclusions

Comparison of the adsorption isotherms for H_2 and D_2 on CMS T3A and nanoporous carbon PCS show that there are significant differences between the isotherms. However, the isotherms overlap when plotted on a surface coverage basis. A virial analysis of the isotherm data indicates that these differences are related to adsorbate−adsorbent interactions which were slightly greater for D_2, while adsorbate−adsorbate interactions were lower for D_2 compared with H_2. The former is attributed to differences in the quantum-statistical mass effect on the vibrational energy levels normal to the surface and the dispersion energy, while the latter is attributed to the higher zero-point energy of H_2. Comparisons of the amounts of D_2 with H_2 adsorbed for specific isotherm points were similar for both CMS T3A (the kinetically selective material for O_2 and N_2), PCS, and G212 (nonselective with very fast adsorption kinetics),[3] indicating no exclusion of either H_2 or D_2 from the porous structures.

The rate constants for adsorption of heavier D_2 on both CMS T3A and PCS are faster than lighter H_2 for the corresponding isotherm pressure increment. The D_2 desorption kinetics are also quicker than the corresponding H_2 kinetics for CMS T3A. The largest k_{D_2}/k_{H_2} ratios were observed for CMS T3A, which has the narrowest porosity, which is kinetically selective material for air separation. These observations are attributed to the higher zero-point energy for H_2 compared with D_2, with H_2 having a

higher effective collision cross section than D_2, producing a higher barrier to diffusion into the porous structures and slower adsorption/desorption kinetics. This is the first experimental observation of kinetic isotope quantum molecular sieving in porous materials. These kinetic characteristics, coupled with the slightly higher amounts of D_2 adsorbed, form the basis of a method for isotope separation at 77 K. This may have advantages over separation at 20 K, which is a particularly energy intensive process.

Supporting Information Available: Adsorption isotherm data are available free of charge via the Internet at http://pubs.acs.org.

References and Notes

(1) *Grand challenge for basic and applied research on hydrogen storage: statement of objectives*; http://www.eere.energy.gov/hydrogenandfuelcells/hydrogen/storage. html#objectives

(2) Zhao, X. B.; Xiao, B.; Fletcher, A. J.; Thomas, K. M.; Bradshaw, D.; Rosseinsky, M. J. *Science* **2004**, *306*, 1012.

(3) Zhao, X. B.; Xiao, B.; Fletcher, A. J.; Thomas, K. M. *J. Phys. Chem. B* **2005**, *109*, 8880.

(4) Beenakker, J. J. M.; Borman, V. D.; Krylov, S. Y. *Phys. Rev. Lett.* **1994**, *72*, 514.

(5) Beenakker, J. J. M.; Borman, V. D.; Krylov, S. Y. *Chem. Phys. Lett*. **1995**, *232*, 379.

(6) Wang, Q.; Challa, S. R.; Sholl, D. R.; Johnson, J. K. *Phys. Rev. Lett.* **1999**, *82*, 956.

(7) Reid, C. R.; Okoye, I. P.; Thomas, K. M. *Langmuir* **1998**, *14*, 2415.

(8) Reid, C. R.; Thomas, K. M. *Langmuir* **1999**, *15*, 3206.

(9) Reid, C. R.; Thomas, K. M. *J. Phys. Chem. B* **2001**, *105*, 10619.

(10) Chagger, H. K.; Ndaji, F. E.; Sykes, M. L.; Thomas, K. M. *Carbon* **1995**, *33*, 1405.

(11) Benham, M. J.; Ross, D. K. *Z. Phys. Chem. Neue Folge* **1989**, *163* (1), 25.

(12) *CRC Handbook of Chemistry and Physics*, 74th ed.; CRC Press: Boca Raton, FL, 1993.

(13) Sing, K. S. W.; Everett, D. H.; Haul, R. A. W.; Moscou, L.; Pierotti, R. A. Rouquerol, J.; Siemieniewska, T. *Pure Appl. Chem.* **1985**, *57*, 603.

(14) Dubinin, M..M.; Radushkevich, L. V. *Dokl. Akad. Nauk. SSSR* **1947**, *55*, 327.

(15) Cazorla-Amorós, D.; Alcañiz-Monje, J.; Linares-Solano, A. *Langmuir* **1996**, *12*, 2820.

(16) Cazorla-Amorós, D.; Alcañiz-Monje, J.; de la Casa-Lillo, M. A.; Linares-Solano, A. *Langmuir* **1998**, *14*, 4589.

(17) Linares-Solano, A, Salinas Martínez de Lecea, C, Alcañiz Monge, J, Cazorla-Amorós, D. *Tanso* **1998**, *185*, 316.

(18) Dubinin, M. M.; Stoeckli, H. F. *J. Coll. Interface Sci.* **1980**, *75*, 34.

(19) Langmuir, I. *J. Am. Chem. Soc.* **1918**, *40*, 1361.

(20) Yaris, R.; Sams, J. R., Jr. *J. Chem. Phys*. **1962**, *37*, 571.

(21) van Dingenen, W.; van Itterbeek, A. *Physica (The Hague)* **1939**, *6*, 49.

(22) Nijkamp, M. G.; Raaymakers, J. E. M. J.; Van Dillen, A. J.; De Jong, K. P. *Appl. Phys. A* **2001**, *72*, 619.

(23) Pang, J.; Hampsey, J. E.; Wu, Z.; Hu, Q.; Lu, Y. *Appl. Phys. Lett.* **2004**, *85*, 4887.

(24) Cole, J. H.; Everett, D. H.; Marshall, C. T.; Paniego, A. R.; Powl, J. C.; Rodriguez-Reinoso, F. *J. Chem. Soc., Faraday Trans. 1* **1974**, *70*, 2154.

(25) Constabaris, G.; Sams, J. R.; Halsey, G. D. *J. Phys. Chem.* **1961**, *65*, 367.

(26) Klafter, J.; Schlesinger, M. F. *Proc. Natl. Acad. Sci.* **1986**, *83*, 848.

(27) Hirschfelder J. O., Curtiss, C. F., Bird, R. B. *Molecular Theory of Gases and Liquids*; Wiley: New York, 1966.

(28) Rao, M. B.; Jenkins, R. G.; Steele, W. A. *Langmuir* **1985**, *1*, 137.

(29) Steele, W. A. *Surf. Sci.* **1973**, *36*, 317.

(30) Loughlin, K. F.; Hassan, M. M.; Fatehi, A. I.; Zahur, M. *Gas Sep., & Pur.* **1993**, *7*, 264.

(31) Stoicheff, B. P. *Can. J. Phys.* **1957**, *35*, 730.

(32) Giauque, W. F. *J. Am. Chem. Soc.* **1930**, *52*, 4816.

(33) Johnston, H. L.; Long, E. A. *J. Chem. Phys.* **1934**, *2*, 389.

(34) Tanaka, H.; Kanoh, H.; Yudasaka, M.; Iijima, S.; Kaneko, K. *J. Am. Chem. Soc.* **2005**, *127*, 7511.

(35) Tanaka, H.; Kanoh, H.; El-Merraoui, M.; Steele, W. A.; Yudasaka, M.; Iijima, S.; Kaneko, K. *J. Phys. Chem. B* **2004**, *108*, 17457.

(36) Challa, S. R.; Sholl, D. S.; Johnson, J. K. *J. Chem. Phys.* **2002**, *116*, 814.

(37) Challa, S. R.; Sholl, D. S.; Johnson, J. K. *Phys. Rev. B* **2001**, *63*, 245419/1.

(38) Sholl, D. S.; Johnson, J. K. *J. Chem. Phys.* **2002**, *116*, 814.

(39) Lu, T.; Goldfield, E. M.; Gray, S. K. *J. Phys. Chem. B* **2003**, *107*, 12989.

(40) Garberoglio, G.; Skoulidas, A. I.; Johnson, J. K. *J. Phys. Chem. B* **2005**, *109*, 13094.

(41) Kumar, A. V. A., Bhatia, S. K. *Phys. Rev. Lett.* **2005**, *95*, 245901.

(42) Webster, C. E.; Drago, R. S.; Zerner, M. C. *J. Am. Chem. Soc.* **1998**, *120*, 5509.

(43) Guillot, B., Guissani, Y. *J. Chem. Phys.* **1998**, *108*, 10162.

(44) Georgiev, P. A.; Ross, D. K.; De Monte, A.; Montaretto-Marullo, U.; Edwards, R. A. H.; Ramirez-Cuesta, A. J.; Adams, M. A.; Colognesi, D. *Carbon* **2005**, *43*, 895.

(45) Grilly, E. R. *J. Am. Chem. Soc.* **1951**, *73*, 5307.